Method for the height measurement of agricultural implements based on variable parameter Kalman filter

Gaolong Chen[1], Xiwen Luo[1,2,3], Lian Hu[1,2,3*], Pei Wang[1,2,3], Jie He[1,2,3], Dawen Feng[1], Weicong Li[1], Jinkang Jiao[1]

(1. *College of Engineering, South China Agricultural University, Guangzhou 510642, China*;
2. *Guangdong Laboratory for Lingnan Modern Agriculture, Guangzhou 510642, China*;
3. *Guangdong Provincial Key Laboratory of Agricultural Artificial Intelligence (GDKL-AAI), Guangzhou 510642, China)*)

Abstract: To improve the GNSS receiver's accuracy, continuity, and stability in measuring the height of agricultural implements, this study proposed a variable-parameter Kalman filter (VPKF) algorithm based on GNSS and accelerometer to estimate the height of the implements optimally. The VPKF was verified, and its accuracy was evaluated by parallel rail platform and field tests. From the parallel rail test results, when the GNSS receiver was in real-time kinematic (RTK) positioning and the time delay of differential correction data (TDDCD) was less than or equal to 4 s, the root mean square error (RMSE) of the VPKF estimation was 9.82 mm. The RMSE of the GNSS measurement was 18.85 mm. When the GNSS receiver lost differential correction data within 28 s, the absolute error of VPKF was less than 30 mm, and the RMSE was 16.93 mm. The field test results showed that when the GNSS receiver was in RTK positioning and the TDDCD was less than or equal to 4 s, the RMSE of VPKF estimation was 13.43 mm, and the GNSS measurement was 14.56 mm. When the GNSS receiver lost differential correction data within 28 s, the RMSE of the VPKF estimate was 15.22 mm. These results show that VPKF can optimally estimate implement height with better accuracy. Overall, the VPKF can obtain a more accurate, continuous, and stable height of the implement, and increase the application scenarios of the GNSS receiver to measure the implement height.

Keywords: agricultural implement, height, Kalman filter, GNSS, accelerometer
DOI: 10.25165/j.ijabe.20241702.8026

Citation: Chen G L, Luo X W, Hu L, Wang P, He J, Feng D W, et al. Method for the height measurement of agricultural implements based on variable parameter Kalman filter. Int J Agric & Biol Eng, 2024; 17(2): 193–199.

1 Introduction

With the development of precision agriculture, agricultural implement active control technology has been applied in all aspects of the crop production process, including profiling control and constant height control. However, there are differences in the detection methods of agricultural implement height corresponding to the two control methods.

Profiling control determines that the height of agricultural implements is measured using terrain or canopy as a reference surface. Nielsen et al.[1] combined ultrasonic and displacement sensors to monitor the depth of the colters from the ground and developed a corresponding control system. Patel et al.[2] used a 2D LiDAR mounted on the sprayer to obtain the height of the citrus canopy to the ground to control the spraying nozzles to optimize spraying applications. Similarly, Dou et al.[3] used ultrasonics to measure the height between the sprayer boom and the wheat stubble canopy to control the height of the sprayer boom during pesticide application. To harvest the optimal height of wild blueberries, Chang et al.[4] used ultrasonic to sense the height of the header relative to the blueberry canopy to adjust the harvester header's height. The height mentioned above measurement methods are suitable for seeding, field management, and harvesting operations but cannot meet the needs of farmland leveling.

Farmland leveling is an essential part of the rice production process, which can save irrigation water[5], reduce the number of chemical fertilizers and pesticides[6], and increase crop yield[7]. However, the unevenness of the bottom layer of the paddy field affects the accuracy of mechanized agricultural work[8], especially for farmland leveling operations, where the motion of the tractor fluctuates greatly[9], resulting in frequent changes in the height of the scraper. Therefore, constant height control technology is widely used in farmland leveling, including laser-controlled and Global Navigation Satellite System (GNSS)-controlled leveling technology, which determines that the height of agricultural implements is measured with a fixed height as a reference plane. Laser-controlled leveling technology uses a laser transmitter installed at a suitable height to emit a rotating laser beam as a reference plane, and a laser receiver fixed on the scraper senses the laser beam signal to obtain the height difference of the scraper relative to this plane[10]. Considering the limited vertical sensing range of the laser receiver, Zhao et al.[11] fused the laser receiver and accelerometer to estimate the implement height when it exceeds the sensing range of the laser receiver. However, the limited

Received date: 2022-11-06 **Accepted date:** 2023-06-11
Biographies: Gaolong Chen, PhD, research interest: agricultural mechanization and automation, Email: dbalong@163.com; **Xiwen Luo**, Professor, research interest: agricultural mechanization and automation, Email: xwluo@scau.edu.cn; **Pei Wang**, Professor, research interest: agricultural mechanization and automation, Email: wangpei@scau.edu.cn; **Jie He**, Professor, research interest: agricultural mechanization and automation, Email: hooget@scau.edu.cn; **Dawen Feng**, MS candidate, research interest: agricultural mechanization and automation, Email: fdw_199701@163.com; **Weicong Li**, MS candidate, research interest: agricultural mechanization and automation, Email: stcmfr_ot@163.com; **Jinkang Jiao**, PhD, research interest: agricultural mechanization and automation, Email: jiaojk320@163.com.
***Corresponding author: Lian Hu**, Professor, research interest: agricultural mechanization and automation. 483 Wushan Road, Tianhe District, Guangzhou, 510642, China. Tel/Fax: +86-20-38676975, Email: lianhu@scau.edu.cn.

transmission distance of the laser transmitter makes the laser leveling technology unable to work in large fields[12]. At the same time, farmers need to manually place the laser transmitter at the proper position and height before the operation, increasing the operation's complexity. To solve those problems, Tang et al.[13] developed a water surface extraction algorithm based on a two-dimensional laser rangefinder and measured the height of the scraper with the water surface as the benchmark, but this measurement method needs to be performed within 10.5-24.0 h after the rotary tillage.

According to the height output by the GNSS receiver in the Real-time kinematic (RTK) positioning, the GNSS-controlled leveling technology sets the height reference plane and calculates the height difference of the scraper relative to the reference plane during the operation. Compared with laser-controlled leveling technology, it can not only operate in fields with large areas and undulating terrain but also has the advantages of simple installation and operation. However, the original GNSS height data has the problems of outliers, high volatility, and insufficient precision. Wang et al.[14] removed outliers from GNSS height data based on an interval estimation algorithm. Hu et al.[15] employed weighted recursive averaging filtering to reduce fluctuations in GNSS height data. Similarly, Xia et al.[16] proposed a five-point cubic smoothing algorithm to enhance the accuracy of GNSS height data. The above filtering algorithm can improve the measurement accuracy of the GNSS receiver but cannot improve the measurement frequency, which is usually only 10Hz. When agricultural machinery is operating at high speed, the lack of measurement frequency can lead to a reduction in the quality of the work. In addition, when the GNSS receiver loses the differential correction data, the measurement accuracy is seriously reduced, and the above filtering algorithm cannot provide centimeter-level measurement accuracy.

This study aimed to propose an improved data processing algorithm based on GNSS and accelerometer, which can improve the accuracy, continuity, and stability of the GNSS receiver in measuring the height of the implement. The method is the basis for efficient and high-quality farmland leveling, especially in paddy fields with uneven bottoms. Further, the algorithm can increase the application scenarios of GNSS in field operations, such as high-standard farmland construction and unmanned agricultural operations.

2 Material and methods

2.1 Global Navigation Satellite System (GNSS)

The GNSS provides position information to GNSS receivers anywhere on or near the Earth where there is an unobstructed line of sight to four or more GNSS satellites. Therefore, GNSS receivers mounted on agricultural implements can measure the height of the implements through the GNSS positioning function. In addition, RTK positioning can correct common errors in the current GNSS receiver based on the differential correction data from a nearby reference station[17], providing centimeter-level accuracy[18]. However, transmitting the differential correction data to the GNSS receiver in real time has the problem of time delay, which affects the positioning accuracy of the GNSS receiver[19]. To make matters worse, when the data transmission between the GNSS receiver and the reference station is unexpectedly interrupted, the GNSS receiver loses the differential correction data, which can seriously reduce the positioning accuracy. Therefore, the GNGGA log output by the GNSS receiver (i70, vertical accuracy in RTK positioning is ±15mm and decreases by 1 mm for every kilometer of distance between the GNSS receiver and the reference station) produced by the CHCNAV (Shanghai, China) was collected to analyze the stability of RTK positioning. Meanwhile, the data transmission between the GNSS receiver and the reference station was interrupted during the acquisition process. After the acquisition, the quality indicator (QI), which represents the positioning status of the GNSS receiver, and the time delay of differential correction data (TDDCD) in the GNGGA log were extracted and plotted in Figure 1.

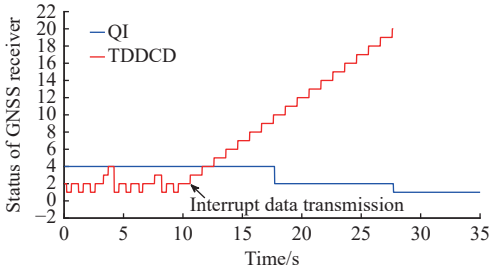

Figure 1 Positioning status of GNSS receiver

As shown in Figure 1, the abscissa represents the sampling time, and the ordinate can define the QI and TDDCD, respectively. The QI of 4, 2, and 1 represent RTK positioning, pseudo-range differential positioning, and single-point positioning. Before interrupting data transmission, the GNSS receiver was in RTK positioning, and the TDDCD was less than or equal to 4 s. However, after the interruption of data transmission, although the GNSS was also in RTK positioning, the TDDCD kept getting larger and exceeded 4 s. When the TDDCD reached 10 s, the GNSS receiver became pseudo-range differential positioning, which can only provide sub-meter-level positioning accuracy[20]. Therefore, when the GNSS receiver was in RTK positioning and the TDDCD exceeded 4 s, it was used as the judgment basis for the GNSS receiver to lose differential correction data.

2.2 Accelerometer

The accelerometer fixed on the implement can output acceleration information at a high frequency to realize the height estimation of the implement. the MTi-300-2A5G4 attitude and heading reference system (AHRS) produced by the Holland XSENS was used to obtain the z-axis free acceleration of the implement. The z-axis free acceleration is the motion acceleration, without the gravity component, expressed in the local reference frame (East-North-Up). Therefore, consistent with the height output by the GNSS receiver based on the World Geodetic System 1984[21], the z-axis free acceleration direction is not affected by frequent changes in the attitude of the implement.

The raw data output by AHRS contains outliers and zero offsets[22]. Therefore, the static free acceleration with a length of about 50 min was collected for preprocessing of the raw data. The outliers are removed using the Hampel filtering algorithm to minimize the impact on the actual data[23]. the filtering equation is shown in Equation (1).

$$a_k = \begin{cases} a_k, & a_k \le |m_k \pm 3\sigma_k| \\ m_k, & a_k > |m_k \pm 3\sigma_k| \end{cases} \quad (1)$$

where, a_k is the acceleration at step k, mm/s^2; subscript k denotes the sampling order (k>3); m_k and σ_k represent the mean and standard deviation of the acceleration of three moments before step k, mm/s^2, respectively, and can be expressed as:

$$m_k = \frac{a_{k-3} + a_{k-2} + a_{k-1}}{3} \quad (2)$$

$$\sigma_k = \sqrt{\sum_{i=1}^{n} \frac{(a_{k-i} - m_k)^2}{3}} (n = 3) \tag{3}$$

The filtered data had a zero offset of −13.80 mm/s². The trending term was extracted and removed using the least square method. The acceleration preprocessing result is shown in Figure 2.

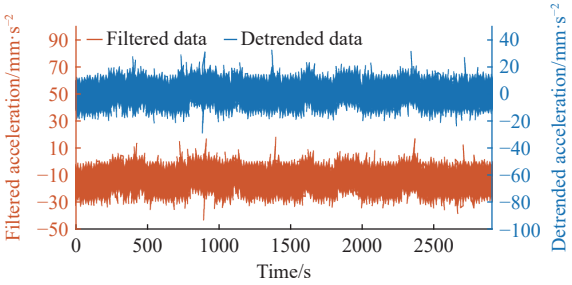

Figure 2 Acceleration preprocessing results

2.3 Variable parameter Kalman filter (VPKF) algorithm based on GNSS and accelerometer

GNSS receivers suffer from insufficient accuracy and undersampling when measuring implement height. To make matters worse, measurement errors can reach sub-meter and meter levels. According to the characteristic that the accelerometer can provide high-frequency height estimation, this paper proposes a variable parameter Kalman filter (VPKF) to fuse the information of GNSS and accelerometer to estimate the height of the implement optimally.

The following equation can express the vertical motion of the implement:

$$S_{k+1} = S_k + \dot{S}_k T + 0.5 a_k T^2 \tag{4}$$

$$\dot{S}_{k+1} = \dot{S}_k + a_k T \tag{5}$$

where, S_k is the actual vertical displacement of the implement, mm; $\dot{S}_k$ is the differential of the displacement to the sampling interval, mm/s; T is the sample interval, s; a_k is the free acceleration of the implement, mm/s²;

The displacement and velocity of the implement as a two-dimensional state vector $\boldsymbol{x_k}$ in the implement's motion state space:

$$\boldsymbol{x}_k = \begin{bmatrix} S_k \\ \dot{S}_k \end{bmatrix} \tag{6}$$

Using Equations (4) through (6), the recurrence equation for the motion state of the implement can be expressed as:

$$\boldsymbol{x}_k = \boldsymbol{A}\boldsymbol{x}_{k-1} + \boldsymbol{B}\boldsymbol{u}_{k-1} + \boldsymbol{w}_{k-1} \tag{7}$$

where, $\boldsymbol{A} = \begin{bmatrix} 1 & T \\ 0 & 1 \end{bmatrix}$; $\boldsymbol{B} = \begin{bmatrix} 0.5 \times T^2 \\ T \end{bmatrix}$; $\boldsymbol{u}_{k-1}$ is control vector; $\boldsymbol{w}_{k-1}$ is process noise;

The measurement equation for the motion state of the implement $\boldsymbol{z}_k$ is,

$$\boldsymbol{z}_k = \boldsymbol{H}\boldsymbol{x}_k + \boldsymbol{v}_k \tag{8}$$

where, $\boldsymbol{H}$=[1 0]; $\boldsymbol{v}_k$ is the measurement noise;

The VPKF of the GNSS and accelerometer is determined as follows:

1) Prior estimation of the system state at step k:

$$\boldsymbol{x}_k^- = \boldsymbol{A}\boldsymbol{x}_{k-1}^+ + \boldsymbol{B}\boldsymbol{u}_{k-1} \tag{9}$$

where, $\boldsymbol{x}_k^-$ is the prior estimation; $\boldsymbol{x}_{k-1}^+$ is the posterior estimation;

2) The prior covariance $\boldsymbol{P}_k^-$ of the error of $\boldsymbol{x}_k^-$ at step k is calculated:

$$\boldsymbol{P}_k^- = \boldsymbol{A}\boldsymbol{P}_{k-1}^+\boldsymbol{A}^{\mathrm{T}} + \boldsymbol{Q}_k \tag{10}$$

where, $\boldsymbol{P}_{k-1}^+$ is the posterior covariance of the error of $\boldsymbol{x}_{k-1}^+$; $\boldsymbol{A}^{\mathrm{T}}$ is the transposed matrix of $\boldsymbol{A}$; $\boldsymbol{Q}_k$ is the process noise covariance matrix, the value of which changes in real-time.

3) Kalman gain $\boldsymbol{K}_k$ at step k is calculated:

$$\boldsymbol{K}_k = \boldsymbol{P}_k^-\boldsymbol{H}^{\mathrm{T}}\left[\boldsymbol{H}\boldsymbol{P}_k^-\boldsymbol{H}^{\mathrm{T}} + \boldsymbol{R}_k\right]^{-1} \tag{11}$$

where, $\boldsymbol{H}^{\mathrm{T}}$ is the transposed matrix of H; $\boldsymbol{R}_k$ is the measurement noise covariance matrix, the value of which is invariable.

4) Posterior estimation $\boldsymbol{x}_k^+$ at step k is calculated and updated:

$$\boldsymbol{x}_k^+ = \boldsymbol{x}_k^- + \boldsymbol{K}_k\left[\boldsymbol{z}_k - \boldsymbol{H}\boldsymbol{x}_k^-\right] \tag{12}$$

5) Posterior covariance $\boldsymbol{P}_k^+$ of the error of $\boldsymbol{x}_k^+$ at step k is calculated and updated:

$$\boldsymbol{P}_k^+ = [\boldsymbol{I} - \boldsymbol{K}_k\boldsymbol{H}]\,\boldsymbol{P}_k^- \tag{13}$$

where, $\boldsymbol{I} = \begin{bmatrix} 1 \\ 1 \end{bmatrix}$ is the unit vector.

The covariance matrixes of process noise $\boldsymbol{Q}_k$ and measurement noise $\boldsymbol{R}_k$ have a significant impact on the results of the Kalman filter. The performance of the Kalman filter is determined by the ratio between $\boldsymbol{Q}_k$ and $\boldsymbol{R}_k$ rather than their respective values[24]. In addition, the time delay and loss of the differential correction data of the GNSS receiver can cause measurement errors to different degrees. Therefore, the algorithm determines the parameter $\boldsymbol{R}_k$ as an invariable value and $\boldsymbol{Q}_k$ as a variable value to achieve its best performance. The parameter $\boldsymbol{R}_k$=1.88×10⁻² is obtained by calculating the root mean square error (RMSE) of the measurement value of the GNSS receiver by subsequent experiments. The adjustment rules of the parameter $\boldsymbol{Q}_k$ are as follows:

$$\boldsymbol{Q}_k = \begin{cases} \boldsymbol{Q}_1 \begin{cases} \text{if QI} = 4 \text{ and TDDCD} \le 4 \\ \text{if QI} = 4 \text{ and TDDCD} > 4 \end{cases} \\ \boldsymbol{Q}_2 \begin{cases} \text{if QI} = 2 \\ \text{if QI} = 1 \end{cases} \end{cases} \tag{14}$$

where, subsequent experiments determine the specific value of $\boldsymbol{Q}_1$ and $\boldsymbol{Q}_2$.

2.4 Algorithm accuracy evaluation and validation

2.4.1 Parallel rail platform test method

A parallel rail test platform was designed to verify the VPKF and evaluate its accuracy. It included a sliding plate, parallel rail, handle, limit stop, GNSS receiver, reference station, AHRS, and linear motion transducer (LMT). The installation positions of the devices are shown in Figure 3, the GNSS receiver and AHRS were mounted on the sliding plate, and the reference station was established near the platform. Meanwhile, The LMT (WXXY15M-400-R, 0-400 mm, linearity of 0.02%) produced by the WXXY MILLAY was installed under the sliding plate to measure the actual displacement of the sliding plate. Since the signal type of the LMT was analog voltage, a ruler (1 mm) was used to calibrate the LMT and the relationship between voltage and displacement can be expressed as Length=121.6Voltage+1.853. The calibration of LMT is shown in Figure 4. The MicroAutoBox II ds1514 produced by dSPACE was used as the data acquisition platform. MicroAutoBox communicated with the computer (Lenovo X220) through the high-speed peripheral bus, and the development environment was Matlab 2016b. The high-performance industrial control board (STM32 F407IGT6) extracted the height, QI, and TDDCD in the GNSS receiver's GNGGA log and then communicated with

MicroAutoBox via RS-232. The AHRS communicated with the MicroAutoBox via RS-232, and the MicroAutoBox's analog-to-digital converter can sample the LMT signal. All the power required for the tests was supplied from the DC-regulated power supply.

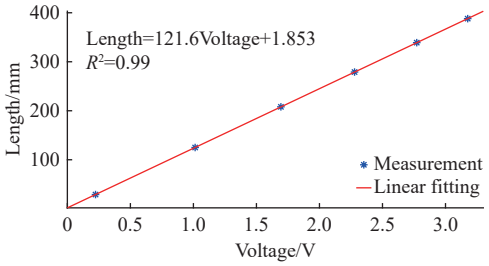

Figure 3 Parallel rail test platform

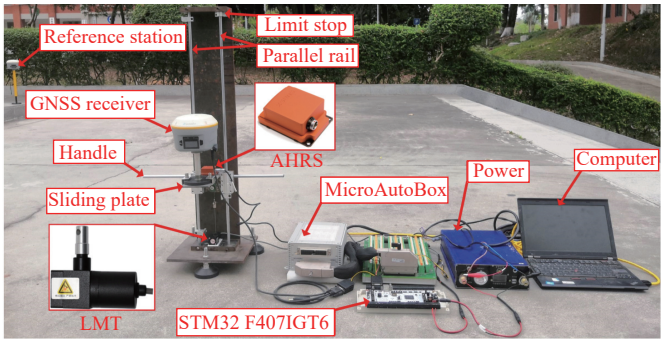

Figure 4 Calibration of the linear motion transducer (LMT)

When the GNSS receiver was in RTK positioning and TDDCD was less than or equal to 4 s, the sliding plate moved to the middle of the parallel guide rail by pulling the handle. The height of the current GNSS receiver output was taken as the reference plane of the sliding plate motion. That was the initial zero position. Therefore, the initial state vector was expressed as:

$$x_k = \begin{bmatrix} S_k \\ \dot{S}_k \end{bmatrix} = \begin{bmatrix} 0 \\ 0 \end{bmatrix} \tag{15}$$

By pulling and pushing the handle to make the sliding plate move reciprocally along the guide rail, the speed range of movement is 0-400 mm/s. MicroAutoBox simultaneously collected height, QI, TDDCD, free acceleration, and voltage data at 50Hz. During the test, the external acceleration introduced by the impact of the sliding plate touching the limit stop was avoided.

2.4.2 Field test method

To verify the performance of VPKF in dynamic scenarios, a field test was carried out on dry land of about 240 m^2 on the experimental farm of South China Agricultural University. As shown in Figure 5, the paddy field leveling machine powered by the Yanmar rice transplanter (2ZGQ-60D) was used as the field test platform. The GNSS receiver, AHRS, and laser receiver (LR4009) were mounted above the scraper. The laser receiver obtains the height difference between the scraper and the laser scanning plane by sensing the position of the laser beam emitted by the laser transmitter (RL-H5A), which measures the actual height of the scraper's movement. Considering the size and arrangement of the photocell units, the laser receiver can sense and output 23 height levels. The height range corresponding to the height level of the laser receiver is listed in Table 1.

As the hardware platform for data acquisition, the computer (HP ZBook 15 G6) was connected to the laser receiver via the PCAN-USB adapter and to the GNSS receiver and AHRS via the RS232-USB adapter. The LabVIEW software was used to write an acquisition program to realize synchronous data acquisition at 50 Hz. When the GNSS receiver was in RTK positioning and TDDCD was less than or equal to 4 s, the laser receiver was in the zero position by adjusting the scraper height. Then, the leveling machine was driven at 1 m/s for testing.

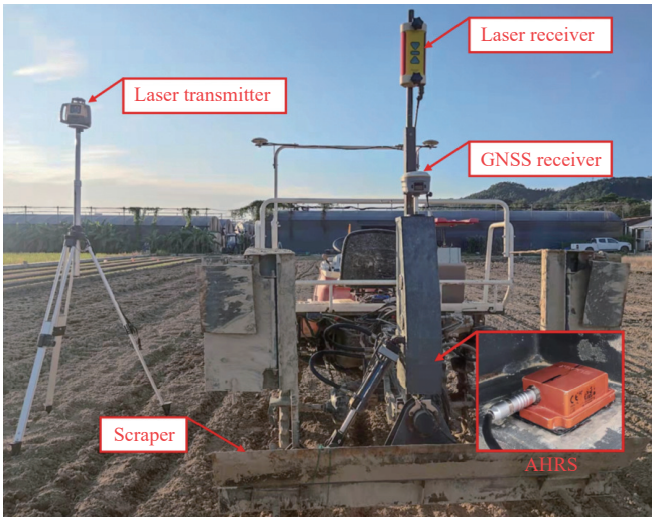

Figure 5 Field test platform

Table 1 Height range corresponding to the height level

Height level/mm	Height range/mm
0	−1.5-1.5
±3	±1.5-±4.5
±6	±4.5-±7.5
±9	±7.5-±10.5
±12	±10.5-±13.5
±15	±13.5-±16.5
±18	±16.5-±19.5
±21	±19.5-±32.5
±33	±32.5-±33.5
±45	±33.5-±62.5
±63	±62.5-±63.5
±81	±63.5-±84.5

3 Results and discussion

3.1 Accuracy of the VPKF methodology

After the test was completed, the collected data was processed and analyzed by Matlab. Since the RMSE of the sliding plate displacement measured by the GNSS receiver was 1.88×10^{-2} m, the parameter $\boldsymbol{R}_k$ was determined to be 1.88×10^{-2}. Meanwhile, the parameters $Q_1 = \begin{bmatrix} 4\times10^{-7} & 0 \\ 0 & 4\times10^{-7} \end{bmatrix}$ and $Q_2 = \begin{bmatrix} 4\times10^{-13} & 0 \\ 0 & 4\times10^{-13} \end{bmatrix}$ were determined by trial and error method. The GNSS measurement and VPKF estimation were compared with the actual displacement measured by the LMT. As indicated in Figure 6a, the GNSS receiver was always in RTK positioning, and TDDCD was less than or equal to 4 s. Both GNSS measurement and VPKF estimation can effectively express the motion displacement of the sliding plate. However, as shown in the local curve in Figure 6b, The GNSS measurement curve changed in a stepped form, caused by each data output from the GNSS receiver being repeated five times to increase the measurement frequency from 10 Hz to 50 Hz. The curve can intuitively reflect the undersampling problems and insufficient precision. In contrast, the VPKF could track the actual displacement curve of the sliding plate, and four heights were recursively acquired between every two heights output by the GNSS receiver,

increasing the measurement frequency from 10 to 50 Hz. Therefore, VPKF can improve measurement frequency and accuracy. As the error distribution is shown in Figure 6c, The GNSS measurement error was significantly larger than the VPKF estimation error. The maximum absolute error (MAE) of the sliding plate displacement measured by the GNSS receiver was 55.61 mm, and the RMSE was 18.85 mm. On the other hand, the MAE of the sliding plate displacement estimated by the VPKF was 25.10 mm, and the RMSE was 9.82 mm. The accuracy was higher than the height output by the GNSS receiver. Therefore, VPKF can improve the accuracy and continuity of measuring the height of the sliding plate.

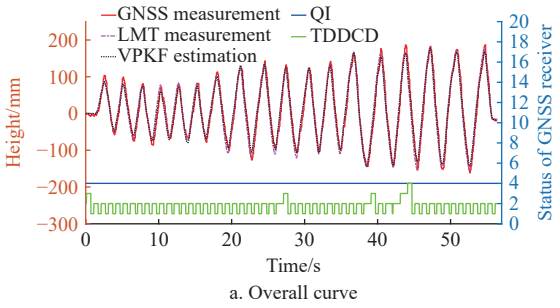

a. Overall curve

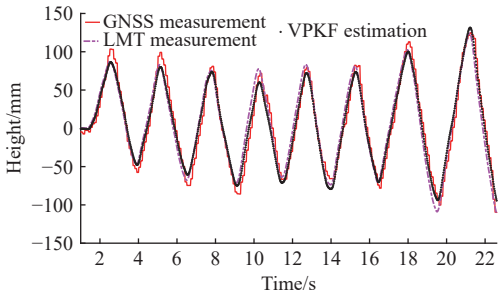

b. Local curve

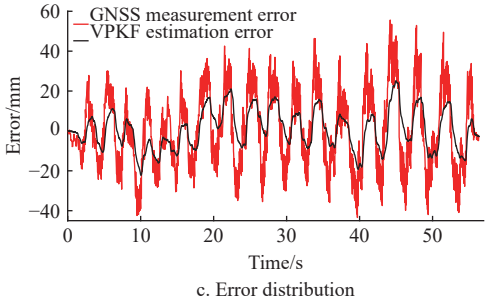

c. Error distribution

Figure 6 Parallel rail test results in RTK positioning

During the test, the data transmission between the GNSS receiver and the reference station was manually interrupted to analyze the performance of VPKF after the GNSS receiver lost differential correction data. As shown in Figure 7a, the measurement accuracy of the GNSS receiver decreased to varying degrees after the loss of differential correction data. According to the "Construction Standards for High Standard of Basic Farmland (TD/T 1033-2012)", the accuracy of farmland leveling should be less than 30 mm. As shown in the error distribution in Figure 7b, the GNSS receiver lost differential correction data at the sampling time of 16.5 s. Before the sampling time of 44.5 s, the absolute error of sliding plate displacement estimated by VPKF was within 30 mm, and then the error gradually increased. The main reason was that the recursive state's weight was significantly increased, and digital integration tended to cause error accumulation. Therefore, the VPKF can guarantee an absolute error of less than 30 mm within 28 s of the loss of differential correction data from the GNSS receiver.

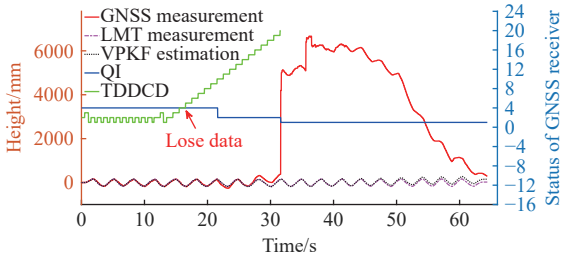

a. Overall curve

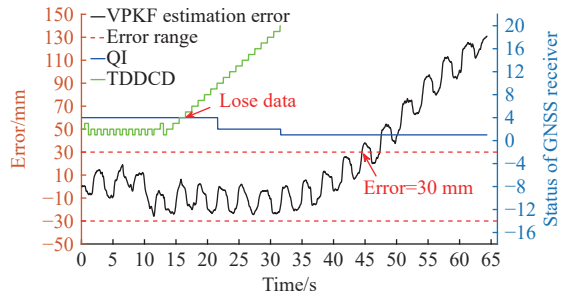

b. Error distribution

Figure 7 Parallel rail test results in losing differential correction data

During the test, data transmission between the GNSS receiver and reference station was manually interrupted and restored to evaluate the accuracy of VPKF within 28 s of the GNSS receiver losing differential correction data. The result is shown in Figure 8a, the GNSS measurement seriously deviated from the actual displacement of the sliding plate during the loss of differential correction data. However, as shown in the local curve in Figure 8b, the VPKF can stably track the actual displacement of the sliding plate. Furthermore, the RMSE of the sliding plate displacement estimated by the VPKF was 16.93 mm. Therefore, the VPKF can stably and accurately estimate the sliding plate displacement within 28 s of the GNSS receiver losing differential correction data.

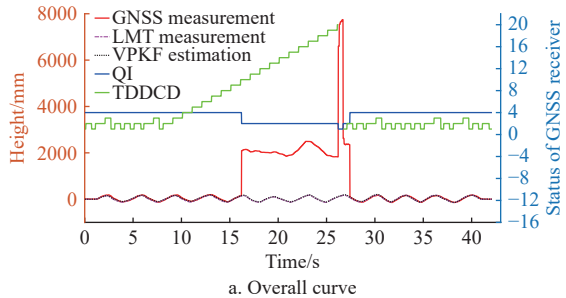

a. Overall curve

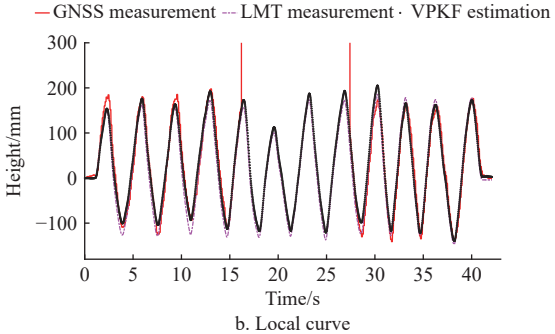

b. Local curve

Figure 8 Parallel rail test results within 28 s of losing differential correction data

3.2 Field validation and performance of the VPKF methodology

Since the noise output by the sensor differed significantly between the parallel rail platform and the field tests, the parameters $Q_1 = \begin{bmatrix} 4.2\times10^{-4} & 0 \\ 0 & 4.2\times10^{-4} \end{bmatrix}$ and $Q_2 = \begin{bmatrix} 4\times10^{-13} & 0 \\ 0 & 4\times10^{-13} \end{bmatrix}$ were adjusted by trial and error method. The error bars drawn by height levels and corresponding deviations represented the actual displacement range of the scraper to analyze the result of the GNSS measurement and VPKF estimation. Figure 9a shows that the GNSS receiver was always in RTK positioning, and TDDCD was less than or equal to 4 s. The GNSS measurement and VPKF estimation mostly passed through the error bars but deviated significantly from the arrow positions' error bars. The main reason was that the scraper movement's displacement exceeded the laser receiver's limited measurement range, which can only output the height levels of ±81 mm. As shown by the local curve Figure 9b, compared with the VPKF estimation, the GNSS measurement exceeded the error bars more times. The main reason was that the high-frequency vibration of the scraper and multipath effect reduced the GNSS receiver's measurement accuracy. Still, the AHRS can provide high-frequency sampling and good measurement accuracy. The MAE of the scraper displacement measured by the GNSS receiver was 76.20 mm, and the RMSE was 14.56 mm. On the other hand, the MAE of the scraper displacement estimated by the VPKF was 61.87 mm, and the RMSE was 13.43 mm. Therefore, VPKF can improve the accuracy and continuity of the scraper displacement measurement in a dynamic operating environment.

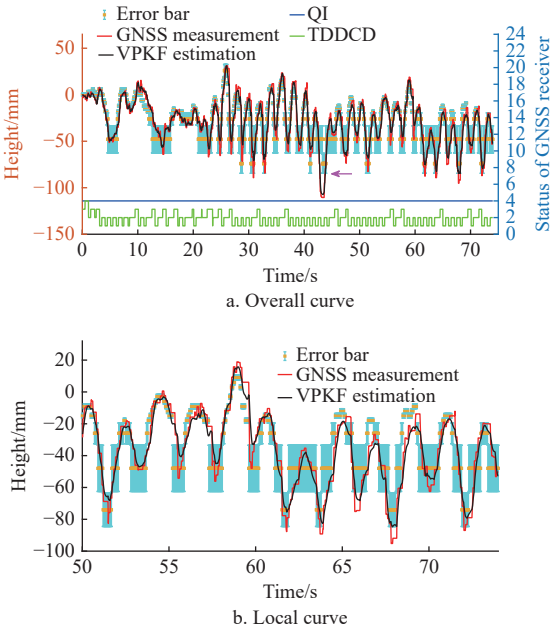

Figure 9 Field test results in RTK positioning

Within 28 s of the GNSS receiver losing the differential correction data, the test results are shown in Figure 10a. The error of the GNSS measurement increased from centimeters to meters as the GNSS receiver lost differential correction data. However, as shown in the local curve in Figure 10b, The VPKF estimation can track the laser receiver's height level output, and the VPKF estimation mostly passes the error bars. Furthermore, the RMSE of the scraper displacement estimated by the VPKF was 15.22 mm. Therefore, VPKF can improve the stability of measuring the movement displacement of the scraper in a dynamic operating environment.

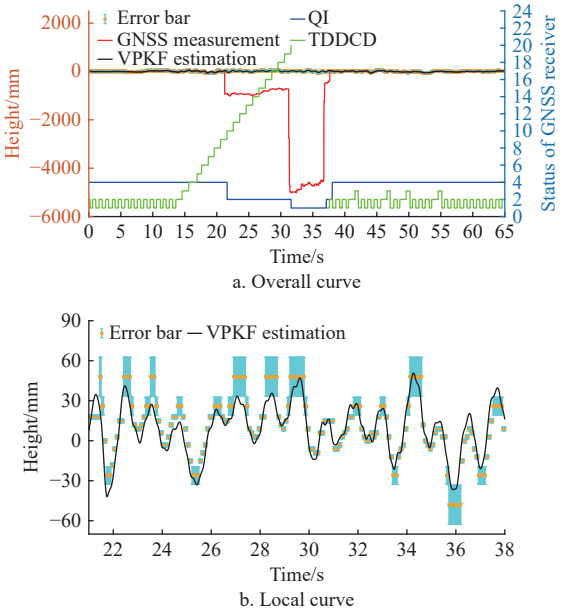

Figure 10 Field test results within 28 s of losing differential correction data

4 Conclusions

In this study, a variable-parameter Kalman filter (VPKF) was proposed to optimally estimate the height of the implement based on GNSS and accelerometer. The parameter change rule was formulated by judging the nodes where the GNSS receiver lost differential correction data.

The parallel rail test results showed that when the GNSS receiver was in RTK positioning and the TDDCD was less than or equal to 4 s, the MAE of VPKF estimation was 25.10 mm and the RMSE was 9.82 mm. Whereas the MAE of GNSS measurement was 55.61 mm and the RMSE was 18.85 mm. When the GNSS receiver lost differential correction data within 28 s, the absolute error of VPKF was less than 30 mm, and the RMSE was 16.93 mm. The field test results showed that when the GNSS receiver was in RTK positioning and the TDDCD was less than or equal to 4 s, the RMSE of VPKF estimation was 13.43 mm, and the RMSE of GNSS measurement was 14.56 mm. When the GNSS receiver lost differential correction data within 28 s, the RMSE of the VPKF estimation was 15.22 mm. These results showed that VPKF can optimally estimate the height of agricultural implements.

Overall, VPKF improves the accuracy, continuity, and stability of GNSS receivers in measuring implement height. Furthermore, VPKF can give farmers enough time for further processing, reducing economic losses and additional labor intensity caused by out-of-control agricultural implementation. At the same time, VPKF increases the application scenarios of GNSS in measuring the height of equipment, such as high-standard farmland construction and unmanned agricultural operations.

Acknowledgements

This research was funded by the Laboratory of Lingnan Modern Agriculture Project (Grant No. NT2021009), National Natural Science Foundation of China (Grant No. 32071913; No. 32101623). The authors also acknowledge the anonymous reviewers for their critical comments and suggestions for improving the manuscript.

[References]

[1] Nielsen S K, Munkholm L J, Lamandé M, Nørremark M, Skou-Nielsen N, Edwards G T C, et al. Seed drill instrumentation for spatial coulter depth measurements. Computers and Electronics in Agriculture, 2017; 141: 207–214.

[2] Partel V, Costa L, Ampatzidis Y. Smart tree crop sprayer utilizing sensor fusion and artificial intelligence. Computers and Electronics in Agriculture, 2021; 191: 106556.

[3] Dou H J, Zhai C Y, Chen L P, Wang S L, Wang X. Field variation characteristics of sprayer boom height using a newly designed boom height detection system. IEEE Access, 2021; 9: 17148–17160.

[4] Chang Y K, Zaman Q U, Rehman T U, Farooque A A, Esau T, Jameel M W. A real-time ultrasonic system to measure wild blueberry plant height during harvesting. Biosystens Engineering, 2017; 157: 35–44.

[5] Bhatt R, Singh P, Hossain A, Timsina J. Rice-wheat system in the northwest indo-gangetic plains of south asia: issues and technological interventions for increasing productivity and sustainability. Paddy and Water Environment, 2021; 19(3): 345–365.

[6] Aryal J P, Mehrotra M B, Jat M L, Sidhu H S. Impacts of laser land leveling in rice-wheat systems of the north-western indo-gangetic plains of India. Food Security, 2015; 7: 725–738.

[7] Jat M L, Gupta R, Saharawat Y S, Khosla R. Layering precision land leveling and furrow irrigated raised bed planting: productivity and input use efficiency of irrigated bread wheat in indo-gangetic plains. American Journal of Plant Sciences, 2011; 2(4): 578–588.

[8] Zhao R M, Hu L, Luo X W, Zhou H, Du P, Tang L M, et al. A novel approach for describing and classifying the unevenness of the bottom layer of paddy fields. Computers and Electronics in Agriculture, 2019; 162: 552–560.

[9] Hu L, Yang W W, He J, Zhou H, Zhang Z G, Luo X W, et al. Roll angle estimation using low cost MEMS sensors for paddy field machine. Computers and Electronics Agriculture, 2019; 158: 183–188.

[10] Zhou H, Hu L, Luo X W, Tang L M, Du P, Mao T, et al. Design and test of laser-controlled paddy field levelling-beater. Int J Agric & Biol Eng, 2020; 13(1): 57–65.

[11] Zhao R M, Hu L, Luo X W, Zhang W Y, Chen G L, Huang H, et al. Method for estimating vertical kinematic states of working implements based on laser receivers and accelerometers. Biosystems Engineering, 2021; 203: 9–21.

[12] Hu L, Xu Y, He J, Du P, Zhao R M, Luo X W. Design and test of tractor-attached laser-controlled rotary scraper land leveler for paddy fields. Journal of Irrigation and Drainage Engineering, 2020; 146(4): 1–8.

[13] Tang L M, Hu L, Zang Y, Luo X W, Zhou H, Zhao R M, et al. Method and experiment for height measurement of scraper with water surface as benchmark in paddy field. Computers and Electronics in Agriculture, 2018; 152: 198–205.

[14] Wang L, Liu G, Liu Y, Li H P. GPS-based land slope leveling technique and its implementation. Journal of Drainage and Irrigation Machinery Engineering, 2013; 31(5): 456–460. (in Chinese)

[15] Hu L, Yang W W, Xu Y, Zhou H, Luo X W, Ke X R, et al. Design and experiment of paddy field leveler based on GPS. Journal of South China Agriculture University, 2015; 36(5): 130–134. (in Chinese)

[16] Xia Y X, Liu G, Kang X, Jing Y P. Optimization and analysis of location accuracy based on GNSS-controlled precise land leveling system. Transaction of the CSAM, 2019; 48(S1): 40–44. (in Chinese)

[17] Wang L, Li Z S, Yuan H, Zhao J J, Zhou K, Yuan C. Influence of the time-delay of correction for BDS and GPS combined real-time differential positioning. Electronics Letters, 2016; 52(12): 1063–1065.

[18] No S, Han J, Kwon J H. Accuracy analysis of network-RTK(VRS) for real time kinematic positioning. Journal of the Korean Society of Surveying, Geodesy, Photogrammetry and Cartography, 2012; 30(4): 389–396. (in Korean)

[19] Refan M H, Dameshghi A, Kamarzarrin M. Improving RTDGPS accuracy using hybrid PSOSVM prediction model. Aerospace Science and Technology, 2014; 37: 55–69.

[20] Rudolph S, Marchant B P, Weihermüller L, Vereecken H. Assessment of the position accuracy of a single-frequency GPS receiver designed for electromagnetic induction surveys. Precision Agriculture, 2019; 20(1): 19–39.

[21] Soycan M. Polynomial versus similarity transformations between GPS and Turkish reference systems. Survey Review, 2005; 38(295): 59–69.

[22] Chen X. Key Technology Research on Attitude Measurement Based on MEMS Sensors. Master's dissertation. Zhejiang: Zhejiang University, 2014, 26p. (in Chinese)

[23] Pearson R K, Neuvo Y, Astola J, Gabbouj M. Generalized hampel filters. EURASIP Journal on Advances in Signal Processing, 2016; Article No. 87. doi: 10.1186/s13634-016-0383-6.

[24] Akhlaghi S, Zhou N, Huang Z Y. Adaptive adjustment of noise covariance in Kalman filter for dynamic state estimation. IEEE Power & Energy Society General Meeting, Chicago: IEEE, 2017; pp.1–5. doi: 10.1109/PESGM.2017.8273755.